

Statics of Pin Corona Charger in Electrophotography

Hiroyuki Kawamoto, Kosuke Takasaki, Hiromu Yasuda and Naohiro Kumagai
Department of Mechanical Engineering, Waseda University
3-4-1, Okubo, Shinjyuku, Tokyo 169-8555, Japan

Abstract

The electrostatic force acting on a pin electrode in a pin-to-plate corona discharge system was measured and numerically calculated by a static unipolar model. The model neglects the effects of diffusion and convection of charged particles. It is assumed that generation of ions takes place on a tip of the pin electrode and that surface electric field is less than the onset field of corona discharge. Numerical calculations were conducted using an iterative finite element method. Calculated voltage-current characteristics of the positive corona qualitatively agreed with the measured result that the corona discharge took place over a threshold voltage and the current was in the order of several ten microamperes. Trichel pulse was observed in case of negative corona and the negative corona current was large compared to the positive corona. Vertical electrostatic force was also measured and calculated. Although extremely small electrostatic pull force was induced if discharge did not take place, the force became repulsive and relatively large when the corona discharge took place. Force in negative corona was almost same with that in positive corona. Calculated force without discharge agreed with the measured but the calculation did not simulate repulsive characteristics at corona discharging. Convection of air must be included in the model. Effect of lean of the pin electrode has been also investigated. The present investigation is expected not only to realize a new ozone-free charger but also to clarify quantitative mechanisms of the bead carry-out in the magnetic brush development subsystem of electrophotography. In addition to these technologies related to the electrophotography, a unique method to drive liquid, named "electrostatic Moses effect," has found and reported. The method is expected to be utilized for a new ink jet printhead.

Introduction

One of the most important issues of electrophotography technology is to reduce ozone emitted by charging and transferring devices, because not only does ozone damage photoreceptors and consequently causes deterioration of images, but it is also harmful for humans.[1] Although the corona chargers,[2] corotrons and scorotrons, have been most widely used in spite of large ozone emission,[3] a new charging device, a biased contact charger roller, has been developed in the late of 1980's to realize extremely low ozone emission.[4, 5] The system consists of a highly electroresistive elastmer roller and a power supply. DC voltage superposed on AC voltage is applied between the photoreceptor drum and the charger roller. The electrical micro-discharge in the vicinity of the nip controls the charging of the photoreceptor.[6] Although ozone is formed in this system, it is extremely small.[7] An ozone filter is usually not necessary to satisfy an environmental standard. Hence it is sometimes termed the virtually ozone free charger. However, the contact charger roller is used only in low-speed machines, because the photoreceptor rapidly wears in this system due to the mechanical contact between the charger roller and the photoreceptor. Alternative discharge current induced by the application of AC voltage accelerates wear of the photoreceptor, because active ions generated in the vicinity of the contact area attack the organic photoconductor. It is believed that the wear mechanism is similar with ion etching. Furthermore it is difficult to realize uniform charging using this charger for high-speed machines.

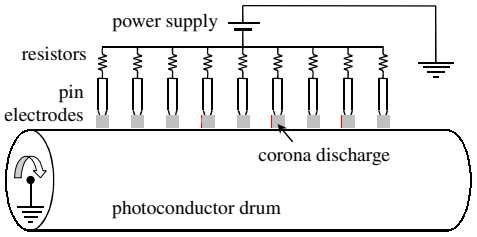

Figure 1. Schematic drawing of new charger with parallel-connected pin electrodes to which high voltage is applied through each resistor.

Another new ozone-free charger was proposed by Furukawa et al.[8, 9] It has pin (saw-tooth) electrodes to which DC high voltage is applied through each resistor as schematically shown in Figure 1. It was confirmed that interposed resistors control sway and dispersion of discharge current from each discharge electrode. Consequently it can uniformly charge the photoreceptor with less discharge current and an amount of generated ozone is less than that of the former charging device with parallel-connected saw-tooth electrodes to which high voltage is directly applied.

Kawamoto[10] has established a theoretical model to calculate ozone emission from this new device applicable for high-speed machines. Results of the calculation were compared with experimental results and some fundamental characteristics and feasibility for the electrophotography charger were discussed. It was cited that the pin charger has a potential to realize virtually ozone-free. However, several subject to be overcome still exist to put the charger to practical use.

Statics and dynamics of the discharge electrode are the other issues of this charger to realize uniform charging, especially in the case that the stiffness of the discharge electrode is low. This is the case when a blush or magnetic bead chains are used as the pin electrodes. The electrode is deformed and/or abnormal vibration is induced by the electrostatic force. A series of investigation has been conducted on the kinetics of a wire-to-plate discharge system to clarify the mechanism of lateral oscillation that is sometimes observed in the corona charger used for a polyester film manufacturing machine.[11] It was reported that in the worst case the vibration caused breakdown of the wire, and then an effective countermeasure was proposed. On the other hand, no systematic study has been performed for the pin-to-plate system except for the measurement of corona-induced force per hanging water drop from a high voltage transmission line and ionic wind in the mechanism of corona induced vibration.[12] In this study, at the first phase of the kinetic investigation, we have study the electrostatic force acting on the pin electrode in a pin-to-plate corona discharge system. The present investigation is expected to be utilized for the design of the new ozone-free charger in electrophotography. In the mean time, a conductive magnetic blush development subsystem in electrophotography is assumed to be a pin-to-plate system; a bead chain corresponds to the pin and photoconductor is the plate electrode. If carrier beads escape from the developer sleeve and adhere to the photoconductor surface, they cause serious image defects. Although many kinds of force, such as magnetic, centrifugal, and Van der Waals, are related to the separation of carrier beads from the chain, the electrostatic force is one of the major factors. The present work is also utilized to the clarification of this phenomenon called "bead carry-out."[2]

Modeling

Because the electric conduction in a field of gas discharge is determined not only by the electrostatic potential ϕ but also by the ionic charge density ρ, two coupled partial differential equations govern the static unipolar field.[13]

$$\nabla \cdot \left(-\omega\rho\nabla\phi\right) = 0 \quad \text{(continuity equation of charge),} \tag{1}$$

$$-\varepsilon_0 \nabla^2 \phi = \rho \quad \text{(Poisson's equation),} \tag{2}$$

where ω is the mobility of ions and ε_0 is the permittivity of free space. Diffusion and convection of charged particles are neglected. Boundary conditions with respect to the potential are simply derived from the fact that the potential difference between the gas discharge electrode and the collecting electrode is equal to the applied voltage V_0.

$$\phi = V_0 \quad \text{at discharge electrode,} \tag{3-1}$$

$$\phi = 0 \quad \text{at collecting electrode.} \tag{3-2}$$

On the other hand, because the boundary condition for the charge density is not known, it is assumed in this model that the electric field E at the surface of the discharging electrode is kept at a constant value E_0, which is equal to the calculated electrostatic field strength determined by the measured corona onset voltage in a coaxial electrode configuration. The adequacy of this assumption has been confirmed in the coaxial cylindrical corona discharge system.[14]

$$E = -\boldsymbol{n} \cdot \nabla\phi \le E_0$$
$$(= 14.55\times10^6 \text{ V/m}) \text{ at discharge electrode,} \tag{4}$$

where $\boldsymbol{n}$ is the unit normal vector to the boundary.

Integration of the current density $\omega\rho E$ over the whole surface of the electrode S yields the total discharge current I.

$$I = \int_S \omega\rho E \, dS \,. \tag{5}$$

The electrostatic force F to the electrode is calculated based on the Maxwell's stress tensor method.

$$F = \frac{1}{2}\varepsilon_0 \int_S E^2 dS \,. \tag{6}$$

After the electrostatic potential ϕ and the ionic charge density ρ are derived from two coupled partial differential equations (1) and (2) satisfying the boundary conditions (3-1), (3-2), and (4), the total discharge current I and the electrostatic force F are determined by the integral equations (5) and (6), respectively, for the given geometry and the applied voltage.

Numerical Method

Figure 2 shows a flowchart of the numerical method. Detailed procedure is as follows:

i) At the first place, the calculation starts with the low applied voltage less than the corona onset voltage. Initial value of ρ is assumed to be uniform and extremely low ($\rho_{initial}$ = 10^{-10} C/m^3).

ii) Two differential equations (1) and (2) are solved independently with respect to ϕ under the boundary condition (3) for the differential equation (1) and the boundary conditions (3) and (4) for the equation (2). Poisson's equation (2) must satisfies the boundary conditions both (3-1) and (4) simultaneously at the discharge electrode. The concrete calculation procedure is that, at the first place, the equation (2) is calculated under the fixed boundary condition (3-1), and if the calculated electric field on the discharge electrode exceeds the threshold E_0, the boundary condition at the corresponding boundary is replaced to (4).

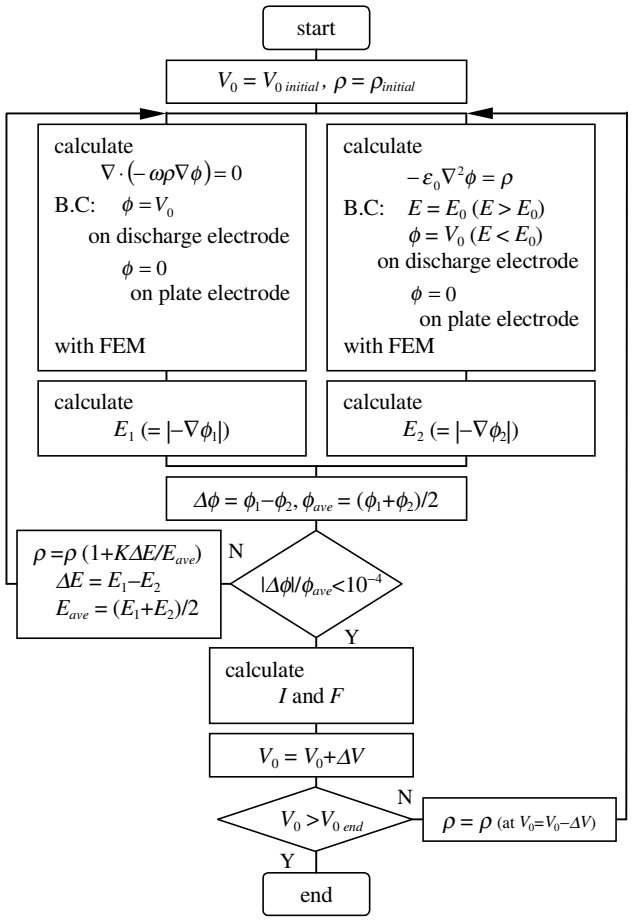

Figure 2. Flowchart of numerical method.

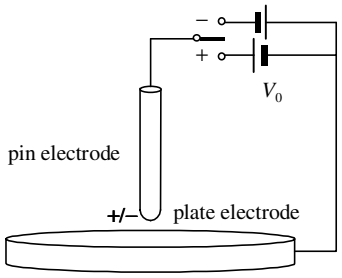

Figure 3. Pin-to-plate electrode system.

iii) Distributions of the electric field, E_1 and E_2, corresponding to two calculated potential distributions, ϕ_1 and ϕ_2, are calculated separately. The subscripts 1 and 2 indicate the continuity equation of charge (1) and the Poisson's equation (2), respectively.

iv) The calculation ii) and iii) are repeated with the revised charge density distribution,

$$\rho_i = \rho_{i-1}\left(1 + 2K\frac{E_1 - E_2}{E_1 + E_2}\right),$$

until $2|\phi_1 - \phi_2|/(\phi_1 + \phi_2) < 10^{-4}$ everywhere, where K is a relaxation coefficient and the subscript i is an iteration step.

v) Total discharge current I and the electrostatic force F are calculated by a simple numerical integration method.

vi) The applied voltage is increased and the procedures ii) to v) are repeated until $V_0 = V_{0end}$. The charge density of the former voltage step is adapted as the initial value to save iteration time.

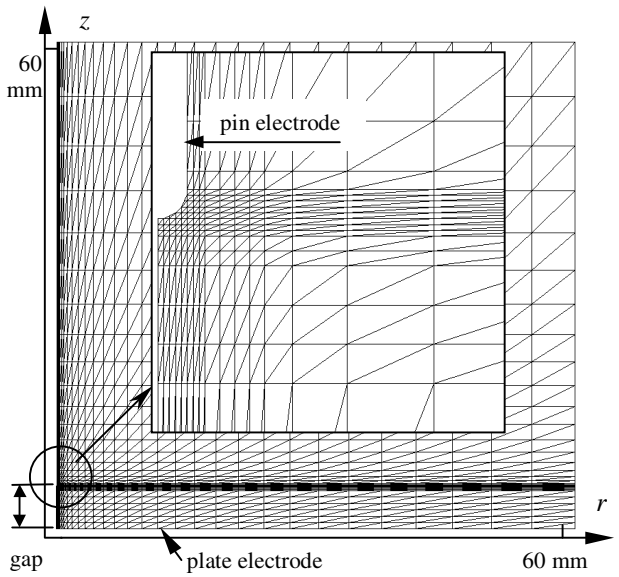

Figure 4. Linear triangular mesh pattern for FEM calculation. (number of nodal point = 1480, number of element = 2805)

The adequacy of the method has been confirmed by comparing numerical solutions with analytical and experimental ones in a coaxial cylindrical field.[14]

The single pin-to-plate electrode, as shown in Figure 3, is simplifies to the two-dimensional coaxial cylindrical system and numerical calculations have been conducted using the finite element method. Figure 4 shows a mesh pattern of the finite element calculation. Instead of the infinite boundaries, large distances from the tip of the pin (r = 60 mm, z = 60 mm) are determined as the insulative boundary. The tip of the pin electrode is assumed to be semispherical and the domain in the vicinity of the tip was finely meshed. The mobility of positive ions ω_+ and negative ions ω_- used for calculations are 1.9×10^{-4} m^2/Vs and 2.5×10^{-4} m^2/Vs, respectively. The adequacy of adapting these values is discussed in the following chapter.

Although it is reported that the preferred relaxation coefficient K is 0.52 for the rapid iteration in the coaxial cylindrical system,[14] it is set to be 0.4 in this calculation to avoid the risk against numerical divergence during the iteration calculation. Number of iteration was several hundreds and the calculation time was about 3 hours for a fixed geometry

and about fifty steps of voltage using a popular DOS/V PC (Pentium III, 500Hz).

Experimental

Figure 5 shows an experimental set-up. A wire made of stainless steel was hung down perpendicular to a steel plate. The diameters of the wire used for experiment were 0.2, 0.3, 0.4, and 0.5 mm. It was connected to the free end of the cantilever plate made of stainless steel. The displacement at the free end of the cantilever was measured by a laser displacement meter (Keyence Corp., LK-2000) and the electrostatic force to the pin was derived multiplying the measured displacement and the stiffness of the cantilever. Two plates were prepared; low stiffness (0.000377 N/mm) and relatively high stiffness (0.00231 N/mm). The former was used to measure extremely low force observed at low applied voltage and the later was for the measurement of relatively large force at corona discharge. The stiffness was statically measured dividing weights put on the free end of the plate by the static displacement measured by the laser displacement meter. Because the electrostatic force to the wire was less than 0.034 gram and thus the axial displacement of the pin was less than 0.17 mm, change of the gap during discharging was negligible compared with the air gap, larger than 3.0 mm. Gap between the wire and the plate was adjusted using a mechanical stage attached at the back of the plate electrode. High voltage was applied to the gap by a DC power supply (Matsusada Precision Inc., HVR-10P (positive) and HVR-10N (negative), 0 ~ ±10 kV adjustable, maximum current 0.15 mA). Voltage was determined by a potentiometer of the power supply and current was measured by the voltage drop in a current-shunt resistor. The surface of electrodes was frequently polished to prevent oxidation and chemical deposition on the tip of the discharge electrode due to gas discharge. Reproducibility of data was confirmed during experiments.

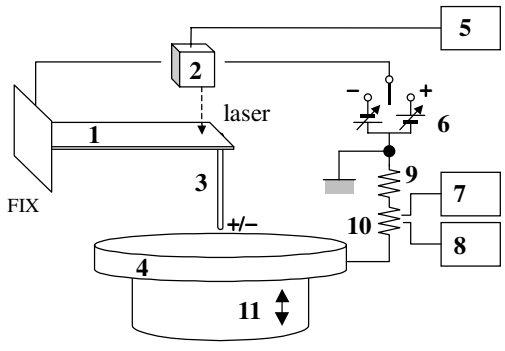

Figure 5. Experimental set-up. (1: stainless steel plate, cantilever, (1) low stiffness T0.1/L140/W10 mm, (2) high stiffness T0.1/L100/W20 mm, 2: laser sensor, 3: pin electrode, SUS304, ϕ0.2, ϕ0.3, ϕ0.4, ϕ0.5 mm, 4: plate electrode, steel, 5: laser displacement meter, 6: DC high voltage power supply, 7: DC volt meter, 8: oscilloscope, 9: resistor, 500 kΩ, 10: shunt resistor, 100 kΩ, 11: mechanical stage)

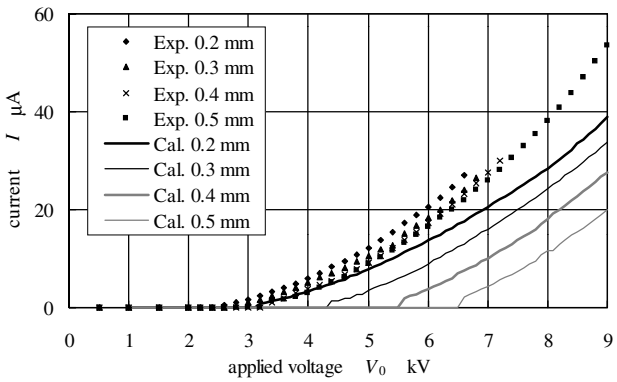

Figure 6. V-I curve in pin-to-plate electrode system. (positive, pin diameter: parameter, 5 mm air gap)

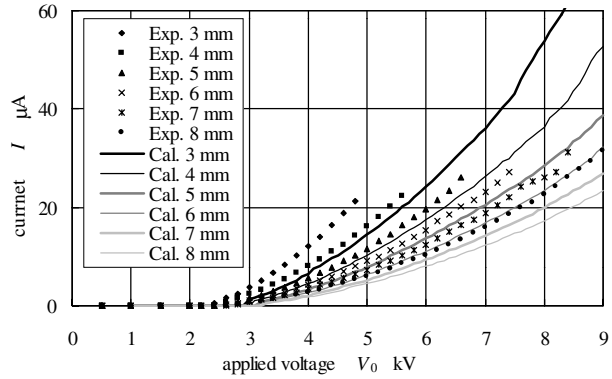

Figure 7. V-I curve in pin-to-plate electrode system. (positive, ϕ0.2 mm pin diameter, air gap: parameter)

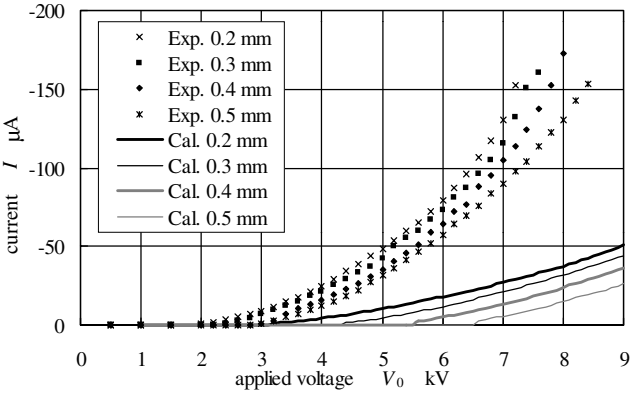

Figure 8. V-I curve in pin-to-plate electrode system. (negative, pin diameter: parameter, 5 mm air gap)

Results and Discussion

Voltage-Current Characteristics

Figure 6 - 9 show measured and calculated voltage-current characteristics. Parameters are; positive or negative, the pin diameter, and the air gap. In any cases fundamental features were similar with those of the corotron. At the voltage lower than the threshold (2 ~ 3 kV), no substantial cur-

rent flowed in the air gap. However, over the threshold voltage, the discharge current in the order of several ten microamperes was measured and at the same time weak luminescence was observed at the tip of the pin electrode. That is, the corona discharge took place. The current and luminescence were stable and the discharge was silent. The corona onset voltage was low and the corona current was high with small pin diameter and small air gap both in positive and negative corona. The onset voltage of the negative corona was almost the same with that of the positive corona but the current was about four times larger than the positive. If the applied voltage was increased, the corona discharge shifted to the spark discharge. (Maximum values of applied voltage plotted in the figures were thresholds of the spark discharge.) Because the spark discharge is non-selfsustaining, the discharge was not continuous but intermittent. When the mode of discharge just changed from the corona to the spark, vertical vibration of the pin electrode took place. Details of this interesting phenomenon will be reported in a separate paper. Since the current was restricted by the maximum capacity of the power supply (0.15 mA), the arc discharge did not take place.

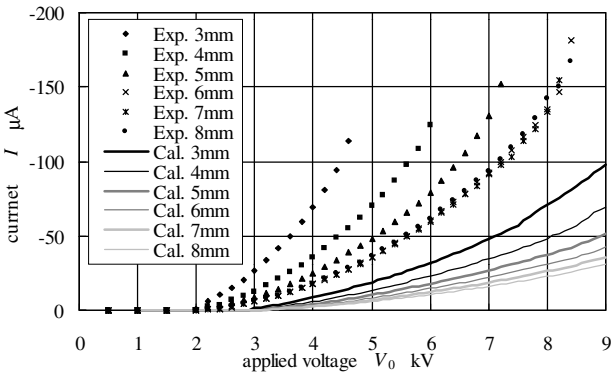

Figure 9. V-I curve in pin-to-plate electrode system. (negative, ϕ 0.2 mm pin diameter, air gap: parameter)

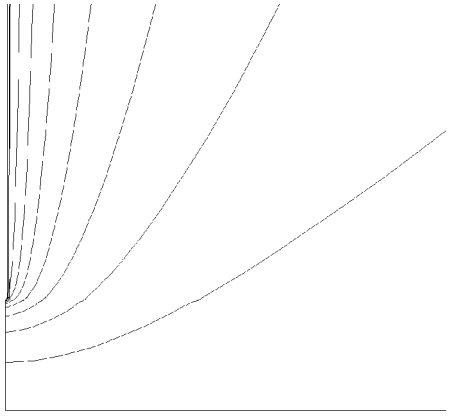

Figure 10. Potential distribution without discharge. (ϕ 0.2 mm pin diameter, 5 mm gap)

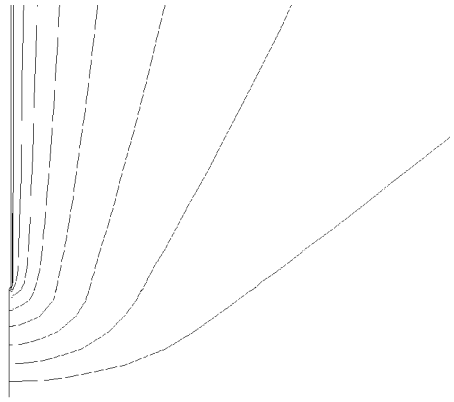

Figure 11. Potential distribution under discharge. (positive, ϕ 0.2 mm pin diameter, 5 mm air gap, V_0 = 4 kV)

Figure 12. Distribution of charge density in the vicinity of the tip of the pin electrode under discharge. (positive, ϕ 0.2 mm pin diameter, 5 mm air gap, V_0 = 4 kV)

The calculated result quantitatively agreed with the measured. At the voltage lower than the threshold, although very low current is calculated depending on the initial value of the charge density, it is negligibly small (in the order of 10^{-12} A). However, when the voltage is further increased and the electric field on the discharge electrode reaches the threshold, current begins to flow because the charge density at the corresponding part becomes large to suppress the increase of the electric field. Thus the electric field at the tip of the pin electrode is maintained the threshold. This is the reason of the experimental evidence that the corona onset voltage was low and the corona current was high with small pin diameter and small air gap. It is well recognized by observing the distributions of the potential and the charge density. Figure 10 shows the potential distribution without discharge and Figure 11 is that under discharge. Curved lines indicate the equi-potential surfaces designating the 10 per cent of the total applied voltage V_0. Figure 12 is the distribution of the charge density in the vicinity of the tip of the pin electrode under discharge. The calculation condition of Figure 12 is common with that of Figure 11. It is clearly understood from these figures that when high voltage is applied, the air is ionized and the charge is yielded in the vicinity of

the tip where the electric field reaches the threshold of the corona onset. Careful comparison of Figure 10 and Figure 11 leads us to recognize that the generation of charge at the tip results in the relaxation of the electric field. The discharge region becomes wide under the high voltage application. This corresponds to the experimental observation that luminescence becomes strong under high voltage.

Calculated results however did not qualitatively agree with the measured that the corona onset voltage and current were not highly dependent of the pin diameter and the current was about four times larger than the positive whereas the calculated was only 1.3 times larger than the positive corona corresponding to the ratio of the positive and negative mobility. It was experimentally clarified that the corona onset voltage was highly dependent to the shape of the pin tip. If a sharp edge existed at the pin tip, the corona discharge took place at low voltage even when the pin diameter was large and on the contrary the onset voltage approached to the calculated for the smooth electrode. Because the pin tip used for experiment was not semi-spherical but somewhat sharp, the corona onset voltage of the actual electrode was lower than that of the ideally smooth electrode. However, the reason of the other discrepancies is not clear. It must be clarified why the model, which was reasonable for the wire-to-plate or coaxial cylindrical systems,13, 14 is not applicable for the pin-to-plate.

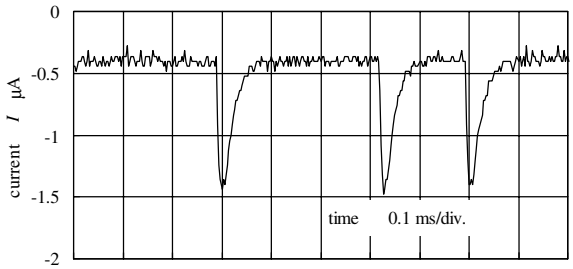

Figure 13. Trichel pulse. (negative, ϕ 0.2 mm pin diameter, 5 mm air gap, V_0 = 3 kV) Vibration of the pin electrode caused fluctuation of pulse frequency. Corona current was measured by the oscilloscope to eliminate Trichel pulse when it took place at the beginning of the negative corona discharge.

In case of the negative corona, one of the reasons of the later discrepancy is the neglect of time-dependent effect of the negative corona in the present model. That is, although Trichel pulse[15] takes place in the pin-to-plate negative corona discharge system as shown in Figure 13, it is not included but assumed to be static. The occurrence of Trichel pulse is one of major differences of the pin-to-plate system to the wire-to-plate or coaxial cylindrical systems. Another possible reason of the discrepancy that the negative current was about four times larger than the positive is due to the estimation of the effective mobility of negative charged media. Although the electric conduction in the positive discharge is solely due to positive ions, not only negative ions but also electrons contribute to the electric conduction in the negative corona. In case of an electron beam printhead it is reported that the charge deposited in a dielectric film is predominantly electrons.[13, 16] Experimental results indicate that about 80 % of the total charge is due to electrons.[16] This is not exactly the case of the present system whose air gap is larger than that of the electron beam printhead, 250 μm. Nevertheless the current may be high even though the rate of electrons is small because the mobility of electron is about 400 times larger than that of the negative ion. A multi-component model must be established to simulate the negative corona current.

Electrostatic Force

Figures 14 and 15 are the measured and calculated electrostatic force to the pin electrode under low applied voltage in the positive and negative discharge, respectively. Measurement was done using the low stiffness cantilever. The force acts to the vertical direction and the repulsive force applied to the upper direction is designated to be positive. Even at the voltage lower than the threshold, small force was induced. It was only in the order of 0.001 gram. The force is proportional to a square of the voltage and independent of positive or negative. The calculated was similar with the measured. However, although the dependence of the air gap was small in the calculation, it was large in the measured. Possible reasons of this disagreement are also the non-spherical configuration of the pin tip and the poor reliability of data at extremely low force.

Over the threshold voltage, the force was *repulsive* and became large, in the order of 0.01 gram, in accordance with the increase of voltage as shown in Figure 16 - 19. It showed little dependence to the air gap, the pin diameter, and the difference of positive or negative corona. On the other hand the calculated force is applied to downward and almost constant with respect to the voltage. This is because it is assumed in the model that the electrostatic field is maintained constant at the surface of the pin electrode during corona discharging and only the discharge area becomes large in accordance with the increase of voltage. The similar characteristic was reported in the wire-to-plate system.[11] However, in the present pin-to-plate system, the calculated was perfectly different with the measured. Preliminary experiment to visualize airflow in the vicinity of the pin electrode suggested that the convection of the air, ionic wind, which is neglected in the model, performed an important role to the kinetics of the electrode. The present simulation model must be refined to include not only time-dependency and multi-component features but also diffusion and convection of gases. Although the force was very small compared with that in the wire-to-plate system, it is large enough to change the form of the blush or magnetic bead chains and it is large in more than two orders of magnitude compared with the magnetic force to carrier beads in the magnetic development subsystem (in the order of 0.1 ~ 1 μN). The electrostatic force is one of the most important factors that affect the bead carry-out.

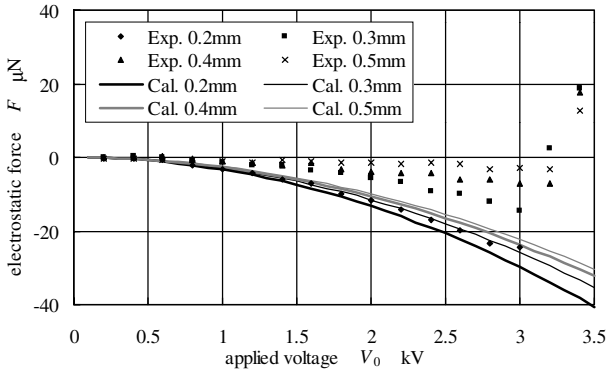

Figure 14. Electrostatic force applied to pin electrode at low voltage. (positive, pin diameter: parameter, 5 mm air gap)

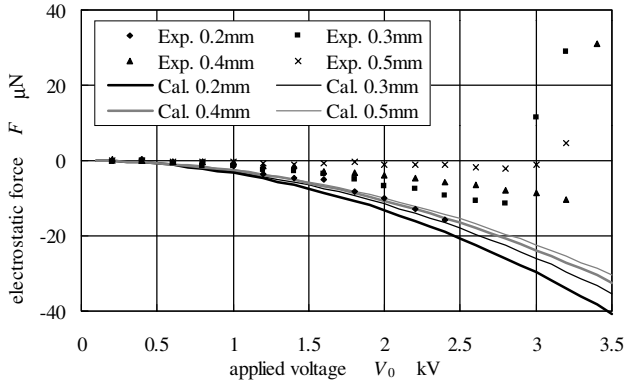

Figure 15. Electrostatic force applied to pin electrode at low voltage. (negative, pin diameter: parameter, 5 mm air gap)

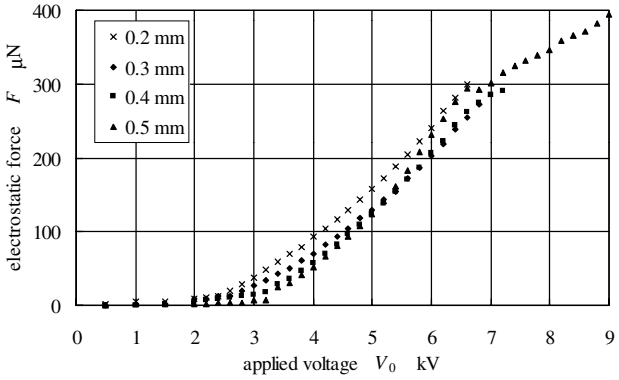

Figure 16. Electrostatic force applied to pin electrode at corona discharge. (positive, pin diameter: parameter, 5 mm air gap)

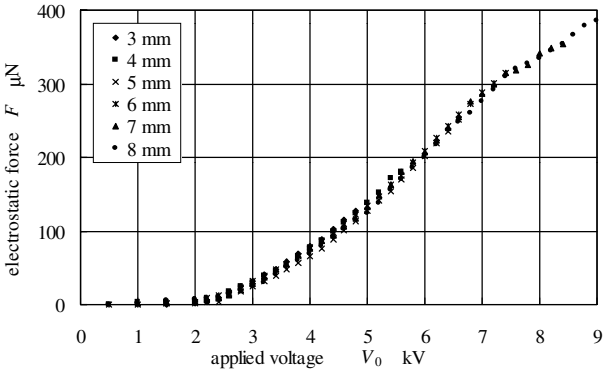

Figure 17. Electrostatic force applied to pin electrode at corona discharge. (positive, ϕ 0.2 mm pin diameter, air gap: parameter)

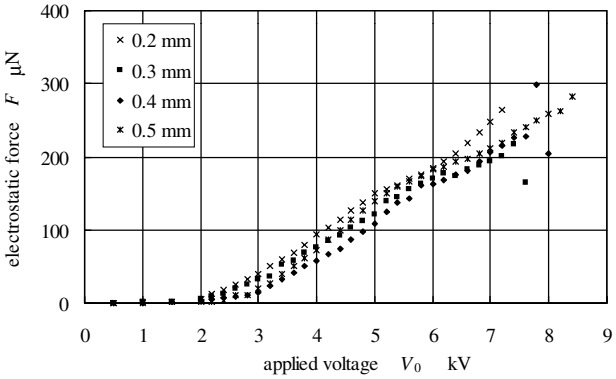

Figure 18. Electrostatic force applied to pin electrode at corona discharge. (negative, pin diameter: parameter, 5 mm air gap)

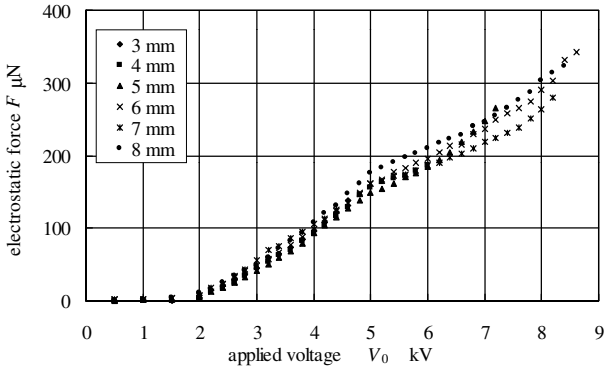

Figure 19. Electrostatic force applied to pin electrode at corona discharge. (negative, ϕ 0.2 mm pin diameter, air gap: parameter)

Effect of Leaning of Pin Electrode

It is impossible in an actual machine to set the pin electrode exactly in right angle to the plate electrode, particularly in the case when a blush or magnetic bead chains are used for pin electrodes. Carrier chains in the two-component magnetic blush development subsystem are also not in right angle to the photoconductor but chains align to the magnetic flux line.[2] Since the system is not symmetry when the pin electrode is not perpendicular to the plate, numerical calculation could not conducted but the effect of leaning of the pin electrode was experimentally investigated. The result is shown in Figure 20 and 21. It is clearly recognized from these figures that the effect of leaning is negligible with respect to both the current and the force even when the lean

was substantially large. This is probably because both the current and the force are determined at the tip of the pin electrode and contribution of the other surface is small.

Concluding Remarks

Statics of the pin electrode in the pin-to-plate system have been investigated to utilize the system for the new ozone free charger and to clarify the fundamental mechanism of bead carry-out in the two-component magnetic blush devel opment subsystem of electrophotography. The following is a summary of the investigation.

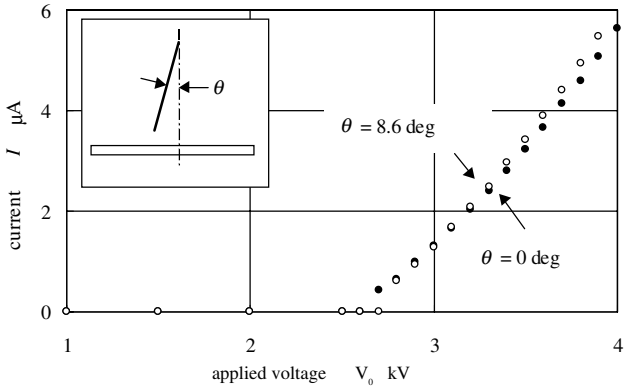

Figure 20. V–I curve in pin-to-plate system in case that the electrodes are not exactly in right angle (positive, ϕ 0.2 mm pin diameter, 5 mm air gap).

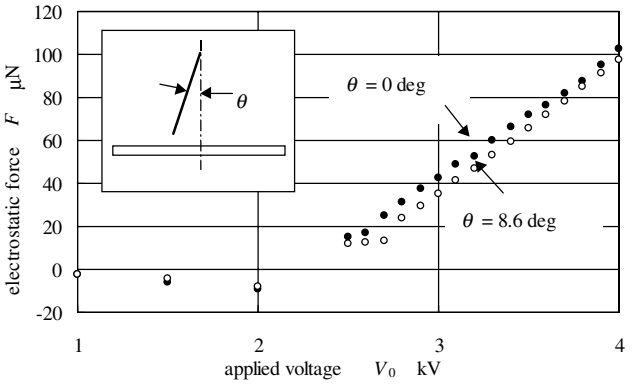

Figure 21. Electrostatic force applied to pin electrode in case that the electrodes are not exactly in right angle (positive, ϕ 0.2 mm pin diameter, 5 mm gap).

Voltage-Current Characteristics.

The corona discharge took place over the threshold voltage. The corona onset voltage is low and the corona current is high under small pin diameter and small air gap both in positive and negative corona. The onset voltage of the negative corona was almost the same with that of the positive corona but the measured current was about four times larger than the positive. Numerical calculation was conducted to calculate the corona current and the electrostatic force. The model is static and unipolar and it neglects the effects of diffusion and convection of charged particles. It is assumed that generation of ions takes place on a tip of the pin electrode and that surface electric field is less than the onset field of corona discharge. Calculated voltage-current characteristics qualitatively agreed with the measured in the positive corona but the calculated negative current was only 1.3 times larger than the positive corona. The reason of the discrepancy is not clear but possible reasons are the neglect of time-dependent effect of the negative corona such as Trichel pulse observed in the negative corona and the neglect of electron conduction in the negative corona.

Electrostatic Force to Pin Electrode.

Although extremely small electrostatic pull force, in the order of 0.001 gram, was induced if discharge did not take place, the force became repulsive and relatively large, in the order of 0.01 gram, when the corona discharge took place. Calculated force without discharge agreed with the measured but the calculation did not simulate repulsive characteristics at corona discharging. Preliminary experiment to visualize airflow in the vicinity of the pin electrode suggested that the convection of the air, ionic wind, must be included in the model.

Effect of Leaning of Pin Electrode.

The effect of leaning of the pin electrode is negligible even when the lean is substantially large (8 deg) probably because both the current and the force are determined almost at the tip of the pin electrode and contribution of the other surface is small.

Acknowledgement

This work is supported by The Iwatani Naoji Foundation's Research Grant.

References

1. T. B. Hansen and B. Andersen, *Am. Ind. Hyg. Assoc. J*, **47**-10, 659 (1986).
2. E. M. Williams, The Physics and Technology of Xerographic Processes, Krieger Publishing Co., Malabar, FL (1993).
3. H. Kawamoto, *J. Imaging Sci. Technol*, **39**-5, 439 (1995).
4. J. Araya, N. Koitabashi, S. Nakamura and H. Hirabayashi, USP 5,164,779 (1992).
5. J. Araya, N. Koitabashi, S. Nakamura and H. Hirabayashi, EP 280 542 (1988).
6. H. Kawamoto and H. Satoh, *J. Imaging Sci. Technol*, **38**-4, 383 (1994).
7. H. Kawamoto, *ibid.*, **39**-3, 267 (1995).
8. K. Furukawa, H. Ishii, K. Shiojima and T. Ishikawa, *Proc. IS&T's Tenth Int. Congress on Advances in Non-Impact Printing Technologies*, 34 (1994).
9. K. Furukawa, H. Ishii, K. Shiojima and T. Ishikawa, *Electrophoto*, **35**-2, 116 (1996).
10. H. Kawamoto, *IS&T's NIP15: Proc. International Conference on Digital Printing Technologies*, 508 (1999).

11. Y. Ito, Dynamics of the Wire Electrode in a System of Wire and Plate Electrodes, Ph.D. Thesis, Keio University (1996).
12. M. Farzaneh and Y. Teisseyre, *IEEE Trans. on Power Delivery*, **3**-3, 1122 (1988).
13. H. Kawamoto and S. Serizawa, *J. Imaging Sci. Technol*, **41**-6, 629 (1997).
14. M. Hattori and K. Asano, *T IEE Japan*, **106**-A-3, 95 (1986).
15. W. L. Lama and C. F. Gallo, *J. Appl. Phys*, **45**-1, 103 (1974).
16. W. J. Caley, W. R. Buchan and T. W. Pape, *J. Imaging Sci. Technol*, **17**-2, 51 (1991).
17. S. Ueno and M. Iwasaka, J. *Appl. Phys*, **75**-10, 7177 (1994).
18. E. Beaugnon and R. Tournier, *Nature*, 349, 470 (1991).

Appendix - Electrostatic Moses Effect -

If the plate electrode made of metal is replaced to water, repulsive reaction force at corona discharge might change the shape of water level. This was confirmed as shown in Figure A1. If the applied voltage was lower than the corona onset threshold, change of water level was invisible to the naked eye. However, over the threshold voltage a relatively large repulsive force was induced and thus the water sank. We named this unique phenomenon "Electrostatic Moses Effect."

A magnetic Moses effect has been reported.[17] It utilizes a high gradient magnetic field[18] that induces magnetic force to diamagnetic fluid, such as the water. A superconducting magnet is necessary to realize the magnetic Moses effect; on the other hand, the electrostatic Moses effect is possible with a conventional power supply. Application of this unique technique is under investigation but it is expected to be utilized for a new ink jet printhead.

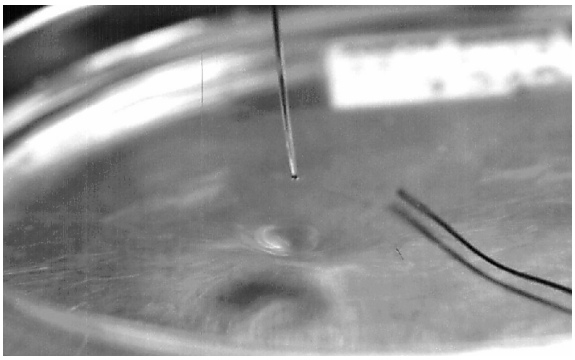

Figure A1. Electrostatic Moses effect. High voltage (~7 kV) is applied between the upper pin electrode (0.5 mm diameter) and the lower water as Moses stretched out his hand over the sea (Exodus 14:21). Cupric sulfate was dissolved in the water to enhance ionic conduction.

Biography

KAWAMOTO, Hiroyuki holds a BS degree in Electrical Engineering from Hiroshima Univ. (1972) and a Dr. degree in Mechanical Engineering from Tokyo Institute of Technology (1983). From 1972 to 1991 he was a Senior Engineer at the Nuclear Division of Hitachi Ltd. In 1991 he moved to Fuji Xerox, and had been engaged in the research of electrophotography as a Research Fellow. In 1999 he left Fuji Xerox and he is now a professor of Waseda Univ. His awards include the Japan Society of Mechanical Engineers Young Scientist Award (1984), the 7th International Microelectronics Conf. Best Paper Award (1992), and the Japan Institute of Invention and Innovation Patent Award (1993). He was selected a Fellow of the IS&T in 1999.